Electronic properties of lanthanide oxides from the GW perspective

Hong Jiang,[1,*] Patrick Rinke,[2] and Matthias Scheffler[2]

[1]*Beijing National Laboratory for Molecular Sciences, State Key Laboratory of Rare Earth Materials Chemistry and Applications, Institute of Theoretical and Computational Chemistry, College of Chemistry and Molecular Engineering, Peking University, 100871 Beijing, China*

[2]*Fritz-Haber-Institut der Max-Planck-Gesellschaft, 14195 Berlin, Germany*

(Received 13 April 2012; published 12 September 2012)

A first-principles understanding of the electronic properties of f-electron systems is currently regarded as a great challenge in condensed-matter physics because of the difficulty in treating both localized and itinerant states on the same footing by the current theoretical approaches, most notably density-functional theory (DFT) in the local-density or generalized gradient approximation (LDA/GGA). Lanthanide sesquioxides (Ln_2O_3) are typical f-electron systems for which the highly localized f states play an important role in determining their chemical and physical properties. In this paper, we present a systematic investigation of the performance of many-body perturbation theory in the GW approach for the electronic structure of the whole Ln_2O_3 series. To overcome the major failure of LDA/GGA, the traditional starting point for GW, for f-electron systems, we base our GW calculations on Hubbard U corrected LDA calculations (LDA + U). The influence of the crystal structure, the magnetic ordering, and the existence of metastable states on the electronic band structures are studied at both the LDA + U and the GW level. The evolution of the band structure with increasing number of f electrons is shown to be the origin for the characteristic structure of the band gap across the lanthanide sesquioxide series. A comparison is then made to dynamical mean-field theory (DMFT) combined with LDA or hybrid functionals to elucidate the pros and cons of these different approaches.

DOI: 10.1103/PhysRevB.86.125115 PACS number(s): 71.10.−w, 71.20.−b, 71.15.−m, 71.27.+a

I. INTRODUCTION

f-electron systems, i.e., materials containing lanthanide or actinide elements, have attracted considerable interest in the past decades as a result of wide industrial application (e.g., industrial catalysis, solid-state lighting, hydrogen storage, permanent magnets, nuclear energy fuels, etc.), and versatile physical and chemical properties (e.g., mixed valence, heavy fermion, high-temperature superconductivity, etc.).[1] From the electronic structure perspective, a typical f-electron system is characterized by the presence of two subsystems: itinerant spd states and highly localized f states. f electrons are presumed to be highly correlated, but can also couple strongly to the spd states. The treatment of f-electron systems therefore poses a great challenge for first-principles modeling due to the difficulty in describing both localized and itinerant states accurately and appropriately in the same theoretical framework.[2]

Lanthanide (or rare-earth) oxides are among the simplest f-electron systems, whose chemical and physical properties are critically dependent on the coupling between localized and itinerant states.[3,4] Besides the fundamental research interest, lanthanide oxides have a wide range of industrial applications. In particular, CeO_2 is important in catalysis, where it is mainly used as support material, but it may also play a more active role.[5] Lanthanide oxides are also considered as promising high-k materials that could replace silica as dielectric in the next generation of field effect transistors.[6,7] Due to their importance in both fundamental research and practical applications, lanthanide oxides have increasingly moved into the focus of first-principles studies in recent years.[8–17]

In this paper we present a systematic investigation of the performance of many-body perturbation theory in the GW approach[18] for the electronic structure of the whole Ln_2O_3 series. In our previous work,[19] we have shown that the G_0W_0 approximation based on Hubbard U corrected density-functional theory in the local-density approximation (G_0W_0@LDA + U) describes the electronic structure of the lanthanide sesquioxide series as measured by direct and inverse photoemission remarkably well. In particular, all main features of the experimental band gaps across the Ln_2O_3 series are well reproduced, and the positions of the occupied and unoccupied f states are qualitatively in good agreement with the experimental conjecture. On the other hand, quantitative differences between G_0W_0@LDA + U and experiment remain, as well as open questions regarding the general performance of GW for lanthanide oxides. In this paper, we present a more detailed investigation of the electronic structure of lanthanide sesquioxides from the GW perspective. Several important issues that were not addressed in our previous work are investigated here, including the influence of the crystal structure, the effects of long-range magnetic order, and the presence of metastable states. Anticipating that the GW@LDA + U approach certainly has its limitation in treating strong interactions between localized f electrons, we make a comparison to dynamical mean-field theory (DMFT)[20,21] for the example of Ce_2O_3. DMFT combined with density-functional theory (DFT) has developed into the method of choice for strongly correlated systems and has been applied to Ce_2O_3 in conjunction with both the LDA and a hybrid functional.[22,23]

The paper is organized as follows. In the next section, we will give a brief overview over first-principles methods to f-electron systems and describe the methods used in this work. Section III is devoted to a detailed discussion of lanthanide oxides in GW@LDA + U. Section V summarizes this work.

II. THEORY AND METHODS

A. f-electron systems from first principles

Kohn-Sham (KS) density-functional theory (DFT) in the local-density or generalized gradient approximations

(LDA/GGA)[24,25]—the state-of-the-art first-principles method for solids[26]—is well known to be inadequate for f-electron systems because of the failure to treat the strong many-body interactions among f electrons properly. For these strongly localized states the self-interaction error becomes particularly severe, which amplifies the infamous band-gap problem of Kohn-Sham DFT. Partially occupied f states are erroneously predicted to cross the Fermi level. As a result many members of the lanthanide sesquioxide family are predicted to be metallic in LDA/GGA and not insulating as in experiment.

The self-interaction error in LDA/GGA can be partly corrected with hybrid functionals that incorporate a certain portion of exact exchange.[27–30] For magnetically ordered phases hybrid functionals can significantly improve the descriptions of the electronic structure of d- or f-electron systems as compared to direct and inverse photoemission experiments.[13,31–33] The exchange contribution in the hybrid functional splits the d or f states that are partially occupied in LDA/GGA into an occupied and an unoccupied manifold in concurrence with experimental observations. However, the dependence on the mixing parameter that controls the amount of exact exchange in the functional remains a concern. The splitting of the partially occupied state can also be achieved by adding a Hubbard U correction to the localized d or f states (LDA/GGA + U).[34,35] Unlike in hybrid functionals, however, the itinerant spd states remain uncorrected in LDA/GGA + U.

Below the Néel temperatures all compounds in the Ln_2O_3 series exhibit antiferromagnetic order and become paramagnetic above. Due to the strong localization of the f states the magnetic coupling between Ln ions is weak and leads to very low Néel temperatures (lower than 10 K).[4] The paramagnetic phase is characterized by an absence of long-range magnetic order and fluctuating local magnetic moments. This phase cannot be described by mean-field theories such as LDA and GGA or even hybrids. Dynamical mean-field theory (DMFT),[20,21] on the other hand, offers a framework to couple a local manifold (e.g., f states) to a mean-field calculation for the extended system dynamically, which captures local magnetic moment fluctuations. Coulomb interactions can in principle be included up to arbitrary order, however, in practice only in the local manifold. Like in LDA/GGA + U, the Hubbard U serves as an input for the interaction strength. In addition, most existing DMFT schemes are coupled (often non-self-consistently) to local or semilocal DFT calculations and the description of the itinerant electrons therefore remains on the level of LDA or GGA.[20,21] Jacob *et al*. recently proposed to combine DMFT calculations with hybrid functionals instead.[22] For Ce_2O_3 they obtained considerably improved results for both the localized f and the itinerant pd states. However, the adequacy of hybrid functionals for itinerant states as well as the uncertainty of choosing the fraction of exact exchange remain a concern.

Many-body perturbation theory in Hedin's GW approximation[18] has become the method of choice for a quantitative description of quasiparticle excitations in sp-bonded solids as measured by direct and inverse photoemission spectroscopy (PES/IPS).[36,37] For d- and f-electron systems an assessment of its adequacy and accuracy is beginning to emerge.[19,38–60] The standard way to apply GW as perturbation to an LDA/GGA ground state (GW@LDA/GGA) is problematic as a result of the pathologies of the LDA/GGA starting point. A simple extension of GW@LDA/GGA is to use LDA/GGA + U as the starting point for GW calculations,[19,61] which can be further justified by the fact that LDA/GGA + U can be derived from GW under certain assumptions.[35,62] Since these assumptions are quite drastic, LDA/GGA + U alone is not expected to deliver accurate electronic band structures for d/f-electron systems. Most importantly, LDA/GGA + U can improve only the description of localized states with strong d/f character; that of itinerant states remains at the LDA/GGA level. On the other hand, by using physically meaningful values of U, GW@LDA/GGA + U gives a balanced description of both itinerant and localized states.[19,62,63]

B. *GW* approximation for quasiparticle excitations

The state-of-the-art first-principles approach to quasiparticle (QP) excitations of real materials is many-body perturbation theory in the GW approximation,[18,36,37,64–69] in which the exchange-correlation self-energy, the central quantity that describes the nonclassical many-body interactions, is a simple product of the one-body Green's function (G) and the screened Coulomb interaction (W). In practice, the most widely used procedure is the so-called G_0W_0 approach, in which both G and W are calculated from the eigenenergies $\{\epsilon_{n\mathbf{k}}\}$ and wave functions $\{\psi_{n\mathbf{k}}\}$ of a single-particle reference Hamiltonian H_0, often that of LDA or GGA. The self-energy then takes the form

$$\Sigma^{\mathrm{xc}}(\mathbf{x},\mathbf{x}';\epsilon) = \frac{i}{2\pi}\int d\epsilon' e^{i\epsilon'\eta} G_0(\mathbf{x},\mathbf{x}';\epsilon+\epsilon')W_0(\mathbf{x}',\mathbf{x};\epsilon'), \tag{1}$$

where $\mathbf{x} = (\mathbf{r},\sigma)$ denotes the collective space and spin coordinate, and η is an infinitesimal positive number.[70] G_0 is calculated from eigenenergies and wave functions of H_0,

$$G_0(\mathbf{x},\mathbf{x}';\epsilon) = \sum_{n\mathbf{k}} \frac{\psi_{n\mathbf{k}}(\mathbf{x})\psi^*_{n\mathbf{k}}(\mathbf{x}')}{\epsilon - \tilde{\epsilon}_{n\mathbf{k}}}, \tag{2}$$

with $\tilde{\epsilon}_{n\mathbf{k}} \equiv \epsilon_{n\mathbf{k}} + i\eta\,\mathrm{sgn}(\epsilon_F - \epsilon_{n\mathbf{k}})$, and W_0 is given by

$$W_0(\mathbf{x},\mathbf{x}';\epsilon) = \int d\mathbf{x}''\varepsilon^{-1}(\mathbf{x},\mathbf{x}'';\epsilon)v(\mathbf{r}''-\mathbf{r}'), \tag{3}$$

where $v(\mathbf{r}-\mathbf{r}') = \frac{1}{|\mathbf{r}-\mathbf{r}'|}$ is the bare Coulomb interaction, and $\varepsilon^{-1}(\mathbf{x},\mathbf{x}'';\epsilon)$ is the inverse dielectric function. The latter,

$$\varepsilon(\mathbf{x},\mathbf{x}',\epsilon) = \delta(\mathbf{x}-\mathbf{x}') - \int d\mathbf{x}'' v(\mathbf{r}-\mathbf{r}'')P_0(\mathbf{x}'',\mathbf{x}';\epsilon), \tag{4}$$

follows from the polarizability,

$$P_0(\mathbf{x},\mathbf{x}';\epsilon) = -\frac{i}{2\pi}\int d\epsilon' e^{\epsilon'\eta} G_0(\mathbf{x},\mathbf{x}';\epsilon+\epsilon')G_0(\mathbf{x}',\mathbf{x};\epsilon'). \tag{5}$$

The QP energies $\epsilon^{\mathrm{QP}}_{n\mathbf{k}}$ are then calculated by treating $\delta\Sigma^{\mathrm{xc}} \equiv \Sigma^{\mathrm{xc}} - V^{\mathrm{DFT}}_{\mathrm{xc}}$ as a perturbation to first order,

$$\epsilon^{\mathrm{QP}}_{n\mathbf{k}} = \epsilon_{n\mathbf{k}} + \mathrm{Re}\langle\psi_{n\mathbf{k}}|\,\Sigma^{\mathrm{xc}}\left(\epsilon^{\mathrm{QP}}_{n\mathbf{k}}\right) - V^{\mathrm{DFT}}_{\mathrm{xc}}\,|\psi_{n\mathbf{k}}\rangle\,, \tag{6}$$

where $V^{\mathrm{DFT}}_{\mathrm{xc}}(\mathbf{r})$ is the exchange correlation potential already included in H_0. Further linearization of Eq. (6) with respect to

the KS energies leads to

$$\epsilon_{n\mathbf{k}}^{\mathrm{QP}} = \epsilon_{n\mathbf{k}} + Z_{n\mathbf{k}}(\epsilon_{n\mathbf{k}})\,\mathrm{Re}\langle\psi_{n\mathbf{k}}|\,\Sigma^{\mathrm{xc}}(\epsilon_{n\mathbf{k}}) - V_{\mathrm{xc}}^{\mathrm{DFT}}\,|\psi_{n\mathbf{k}}\rangle \equiv \epsilon_{n\mathbf{k}} + Z_{n\mathbf{k}}(\epsilon_{n\mathbf{k}})\delta\Sigma_{n\mathbf{k}}(\epsilon_{n\mathbf{k}}), \quad (7)$$

where $Z_{n\mathbf{k}}(E)$ is the QP renormalization factor given by

$$Z_{n\mathbf{k}}(E) = \left[1 - \left(\frac{\partial}{\partial\epsilon}\mathrm{Re}\langle\psi_{n\mathbf{k}}|\,\Sigma^{\mathrm{xc}}(\epsilon)\,|\psi_{n\mathbf{k}}\rangle\right)_{\epsilon=E}\right]^{-1}. \quad (8)$$

For sp semiconductors it has been demonstrated that considerable improvement over G_0W_0 can be obtained by partial self-consistency[67,71] without introducing too much computational overhead. In the so-called eigenvalue self-consistent or GW_0 approach the energy denominator in the Green's function [Eq. (2)] is updated by the $\epsilon_{n\mathbf{k}}^{\mathrm{QP}}$'s, but W remains unchanged. For many semiconductors, it has been found that the GW_0 approach gives band gaps in good agreement with experiment,[57,71] and its overall performance is comparable to that of the much more sophisticated quasiparticle self-consistent GW (QSGW) scheme (in which the most optimum noninteracting system is constructed self-consistently) once an electron-hole vertex is added to W in QSGW.[72] In this work, we mainly use GW_0 based on LDA + U (see below) to investigate the electronic band structures of lanthanide sesquioxides. We note that a comprehensive assessment of self-consistency for f-electron systems is in order, which, however, is beyond the scope of the present work, and will be left for future investigations.

C. *GW*@LDA + *U* method

For systems with partially occupied d/f shells, the severe self-interaction error of LDA often results in an inadequate description, leading to qualitatively wrong metallic ground states for many insulating systems. A simple and effective approach to correct for this is to introduce a local, Hubbard-like correction, characterized by the on-site Coulomb interaction (U), which pushes occupied d/f states towards lower energy (large binding energy), and unoccupied d/f states towards higher energy. This approach, termed LDA + U, can be "derived" from the GW method under the following assumptions:[35,62] (1) the frequency dependence of the screened Coulomb interaction can be neglected (static approximation); (2) quasiparticle corrections are necessary only for localized states, and therefore itinerant states are still treated at the LDA level; and (3) all Coulomb matrix elements involving the overlap of localized states and itinerant states are neglected. Obviously, LDA + U is a rather crude approximation to GW and can improve only the description of states with strongly localized d/f character.[62] Itinerant states are still treated at the LDA level. Therefore LDA + U is not expected to provide an accurate description of d/f-electron systems on its own. However, since LDA + U corrects the major failure of LDA for d/f-electron systems, it is likely to be able to serve as a good starting point for G_0W_0 and GW_0 calculations.[19,61–63]

One of the main concerns when applying LDA/GGA + U to d/f-electron systems is that the results might depend on the value of U quite sensitively. As a parameter characterizing the strength of the on-site Coulomb interaction, U is not universal but system dependent. In practice, U is often used as an adjustable parameter that is determined by fitting experimental data. Treating U as an empirical parameter might bring the risk that important physics could be masked as a result of using a physically unfounded U. There have been long-standing efforts to develop first-principles approaches that determine U without experimental input, including most notably the supercell constrained DFT (cDFT) method,[34,73,74] and the constrained random-phase approximation approach.[75,76] On the other hand, we note that all these so-called first-principles approaches, although nonempirical in the sense that no experimental information is needed, can depend on factors that are not uniquely defined, e.g., the projectors that determine the local correlated subspace. Some degree of uncertainty is always involved in the U's calculated by these approaches, which essentially gives a "physical" range of U's. In the case of lanthanide elements, this physical range is estimated to be 5–7 eV based on different cDFT calculations.[77]

In LDA/GGA + U, the U correction appears in the single-particle equation as a linear term. Therefore the electronic band structures from LDA + U, including, in particular, the positions of occupied and unoccupied f states, can strongly depend on the precise value of U. On the other hand, in GW calculations based on the LDA/GGA + U, the dependence of quasiparticle energies on U is implicit, and therefore weaker in most cases compared to that in LDA + U.[62] A precise determination of U is therefore not crucial in GW based on LDA + U as long as U falls in the physical range, as we will demonstrate later.

D. Computational details

In this work we use G_0W_0 and GW_0 based on LDA + U to investigate the electronic band structures of lanthanide sesquioxides (Ln_2O_3). All LDA + U calculations are performed using the WIEN2K package[78] in which the Kohn-Sham equations are solved in the full-potential linearized augmented plane wave (FP-LAPW) approach.[79] We use the following parameters for the FP-LAPW basis: Muffin-tin (MT) radii R_{MT} were set to 2.15 and 1.96 Bohr for lanthanide and oxygen atoms, respectively. Kohn-Sham wave functions are expanded by atomiclike basis functions with angular quantum number l up to $l_{\max} = 10$ in the MT spheres, and by plane waves with the energy cutoff determined by $RK_{\max} \equiv \min R_{\mathrm{MT}} \times K_{\max} = 8.0$ in the interstitial region. The potential and electron density are expanded in lattice harmonics with angular momenta up to $l_{\max} = 4$ within the MT spheres, and by plane waves in the interstitial region. For LDA + U calculations, the double counting correction is treated in the fully localized limit (FLL).[34,80] Unless stated otherwise, we use $U = 5.4$ eV for the whole series of lanthanide oxides.[19]

GW calculations were performed using the FHI-gap (Green function with augmented plane waves) package, a recently developed all-electron GW code interfaced to WIEN2K.[19,62,81,82] The GW self-energies are calculated on a $3 \times 3 \times 2$ **k** mesh. Unoccupied states with energy up to ~270 eV are taken into account. The frequency dependence is treated on the imaginary axis and analytical continued to the real axis by means of a two-pole fit.[82,83] Densities of states (DOS) are calculated using $12 \times 12 \times 6$ **k** points in the Brillouin zone. In the GW case, DOS are obtained from GW quasiparticle energies, first calculated on the sparse **k** mesh and then interpolated to the fine **k** mesh using the Fourier interpolation technique.[84,85] We note

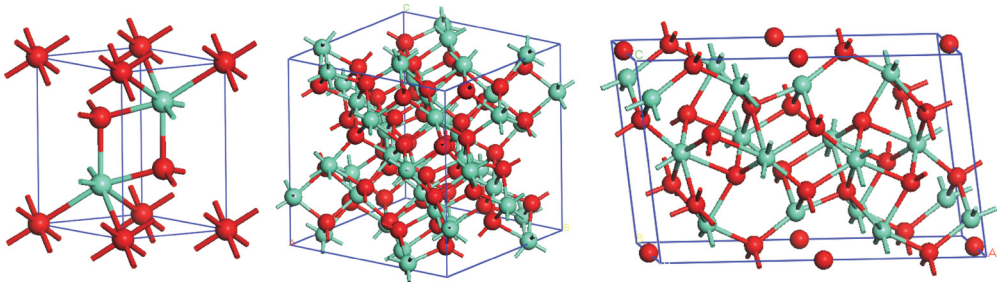

FIG. 1. (Color online) Crystal unit cells of hexagonal, cubic, and monoclinic structures taken by the Ln_2O_3 series.

that the computational parameters used in this work, which are in general more accurate, are slightly different from those used in our previous work,[19] and therefore some quantities are slightly different from those that were already reported in Ref. 19.

Recently it was found that for the semicore d-electron compound ZnO the accuracy of unoccupied states in the LAPW representation can have a significant influence on the GW results, and a large number of additional local orbitals (LOs) are needed to converge the band gap.[86] In contrast, a much weaker influence was previously found for Si (∼0.03 eV for the band gap).[87] Whether this is a general feature of LAPW-based GW calculations for d- or f-electron systems is still an open question. In this work we use the "standard" LAPW basis. To improve the description of unoccupied states,[82,86] we include additional LO basis functions at an energy of 1.0 Ry for $l = 2$ and 3 for lanthanide atoms and $l = 1$ and 2 for oxygen.

III. RESULTS AND ANALYSIS

A. Crystal structures

Lanthanide sesquioxides occur in three stable structures at ambient pressure:[4] (1) a hexagonal structure of $P\bar{3}m1$ symmetry (space group number 164) with one formula unit per unit cell (A form); (2) a monoclinic structure of $C12/m1$ symmetry (space group number 12) with six formula units per cell (B form); and (3) a cubic bixbyite structure of $Ia\bar{3}$ symmetry (space group number 206) with eight formula units per cell (C form). The unit cells of the three structures are illustrated in Fig. 1. Light lanthanide sesquioxides (Ln = La, Ce, Pr, and Nd) usually adopt the A form, heavy lanthanide sesquioxides take the C form, and the intermediate ones (Ln = Pm, Sm, Eu, and Gd) can exist in any of the three forms. The bixbyite structure can be obtained by taking a $2 \times 2 \times 2$ supercell of LnO_2 in the cubic unit cell of the fluorite structure and then removing 1/4 of the oxygen atoms along the [1, 1,1] direction.[3,4] The local environment of each Ln atom is slightly different in the three polymorphs.[3,88] In the A-type (hexagonal) structure, each Ln atom is coordinated by seven oxygen atoms with a distorted capped octahedral geometry. In the cubic C-type structure, all Ln atoms are coordinated by six oxygen atoms. The monoclinic B structure can be regarded as a mixture of the hexagonal and cubic phases with both octahedral and monocapped trigonal prismatic coordination.

The energetic and structural properties of Ln_2O_3 in different polymorphic phases including their relative stability have been systematically studied,[14–17] but the influence of the crystal structure on the electronic properties has not been investigated, as far as we know. Common practice in GW studies of polymorphic materials is to perform GW calculations only for the simplest structures and then to add the GW corrections to the LDA or GGA description of more complex structures.[89,90] The validity of this approximate treatment depends on how sensitively the GW corrections depend on the atomic structure. In previous work for ZrO_2 and HfO_2,[91] and liquid water,[92] it was found that the electronic structure at the LDA/GGA level depends strongly on the atomic structure, whereas the GW corrections are rather insensitive. For Ln_2O_3, a direct comparison of electronic properties of different phases at the GW level is unfortunately not feasible at the moment, because G_0W_0 calculations for the monoclinic or bixbyite structures are computationally not tractable. We therefore investigate the influence of the atomic on the electronic structure at the LDA + U level.

In Fig. 2, we take Eu_2O_3 as an example, and compare the density of states in different phases (all with ferromagnetic order). Qualitatively, the three phases have very similar electronic band structures: the occupied f (f^{occ}) states fall below the O-2p valence bands, spin-up (majority) unoccupied f (f^{un}) states fall in between the O-2p valence and Eu-5d conduction bands, and the spin-down (minority) f^{un} states

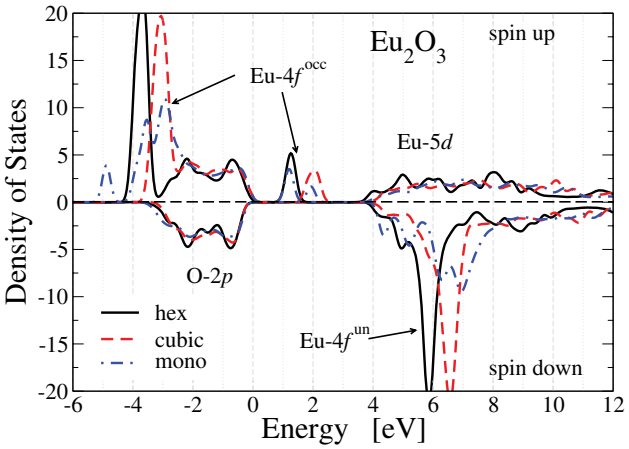

FIG. 2. (Color online) Density of states of Eu_2O_3 in different crystal structures calculated by LDA + U. For the hexagonal phase, we use the structural parameters determined by the linear extrapolation of those of early Ln_2O_3 as explained in Sec. III A. For the monoclinic and cubic bixbyite phases, we use experimental structures from Refs. 93 and 94, respectively.

overlap with the Eu-5d conduction bands. Quantitatively, however, the positions of $f^{\rm occ}$ and $f^{\rm un}$ states are noticeably different in different phases. In addition, due to the different crystal symmetry, the f states exhibit a different crystal-field splitting. In the hexagonal and cubic phases $f^{\rm occ}$ states form a single peak below the O-2p valence band. In the hexagonal face this $f^{\rm occ}$ peak lies ∼0.7 eV lower in energy than in the cubic phase. The monoclinic phase has the lowest symmetry. As a result, the $f^{\rm occ}$ states produce three peaks. The two peaks at higher energy overlap with the O-2p valence band, similar to those in the cubic phase. The third peak is well separated from the others, falling at energy that is ∼1.0 eV lower than the $f^{\rm occ}$ peak in the hexagonal phase. For unoccupied states, the $f^{\rm un}$ states of the majority spin form a single peak in the hexagonal and cubic phases centered at 1.3 and 2.0 eV, respectively, and at almost the same positions the monoclinic phase has two $f^{\rm un}$ peaks. This is consistent with the fact that the monoclinic phase contains two types of Eu atoms that are coordinated to seven and six oxygen atoms, similar to those in the hexagonal and cubic phases, respectively. The $f^{\rm un}$ states in the spin-minority channel also differ in different phases, and once again the features of the monoclinic phase are a mixture of those of the hexagonal and cubic phases. On the other hand, features arising from itinerant states (O-2p and Eu-5d) are very similar in the three phases. The p-d gaps of spin majority (minority) in the hexagonal, monoclinic, and cubic phases are 3.50 (4.02), 3.90 (4.32), and 3.63 (3.88) eV, respectively.

The comparison in Fig. 2 illustrates that the overall features are similar in the different phases, despite the noticeable effect of the local coordination on the band structure. Since in this work we are mainly interested in systematic trends across the Ln_2O_3 series, we will therefore always use the simple hexagonal structure for further investigations. The influence of the crystal structure should, however, be borne in mind when comparing our theoretical results to experimental data.

The hexagonal structure is characterized by four structural parameters: lattice constants a and c and the internal coordinates of Ln ($u_{\rm Ln}$) and O ($u_{\rm O}$). For La_2O_3, Ce_2O_3, Pr_2O_3, Nd_2O_3, and Pm_2O_3, we use experimental hexagonal structural parameters from Ref. 4. For the remaining members of the series, we obtain the lattice constants a and c by constructing the hexagonal structure with the same volume per chemical formula as the experimental cubic structures.[4] The hexagonal lattice constants used in this work are collected in Table I.

TABLE I. The band gaps (in units of eV) of the Ln_2O_3 series in LDA + U, G_0W_0, and GW_0 are compared to experimental values. Unless stated otherwise, most of the experimental data are obtained from optical absorption (Ref. 104). Lattice constants (a, c in units of Bohr) of the hexagonal structures used in this work are also collected. The crystal structures of the samples used in the experimental measurements is often not reported. However, most likely the most stable form, i.e., hexagonal for La_2O_3 to Nd_2O_3 and cubic bixbyite for Sm_2O_3 to Lu_2O_3, will be present (the intermediate members may also take the monoclinic structure). See also Sec. III A for more in-depth discussion.

Ln_2O_3	LDA + U	G_0W_0	GW_0	Expt.	a, c
La_2O_3	3.76	4.95	5.24	5.55[a], 5.34[b], 5.3[c]	7.440, 11.583
Ce_2O_3	2.24	1.50	1.29	2.4[a]	7.351, 11.452
Pr_2O_3	3.17	2.86	2.82	3.9[a], 3.5[b]	7.289, 11.369
Nd_2O_3	3.69	4.50	4.70	4.7[a] 4.8[b]	7.236, 11.333
Pm_2O_3	3.35	5.25	5.41		7.185, 11.251
Sm_2O_3	2.15	4.38	5.22	5.0[a]	7.416, 11.569
Eu_2O_3	1.28	2.77	3.48	4.4[a]	7.371, 11.490
Gd_2O_3	3.58	4.89	5.30	5.4[a]	7.335, 11.443
Tb_2O_3	3.34	3.81	3.74	3.8[a]	7.279, 11.355
Dy_2O_3	3.47	4.41	4.24	4.9[a]	7.236, 11.289
Ho_2O_3	3.05	4.68	5.12	5.3[a]	7.196, 11.225
Er_2O_3	2.69	4.78	5.22	5.3[a], 5.49[b]	7.155, 11.162
Tm_2O_3	1.73	4.73	5.15	5.4[a], 5.48[b]	7.115, 11.099
Yb_2O_3	1.25	3.23	4.70	4.9[a], 5.05[b]	7.082, 11.047
Lu_2O_3	3.18	4.66	4.99	5.5[a], 5.79[b], 4.89[d], 5.8[e]	7.049, 10.997

[a]Reference 104.
[b]Reference 105.
[c]Reference 106.
[d]Reference 107.
[e]Fundamental band gap from internal photoemission spectroscopy in Ref. 107.

B. Effects of magnetic order

Except for La_2O_3 and Lu_2O_3 with empty and fully occupied f shells, all members of the Ln_2O_3 series exhibit a local magnetic moment arising from the localized f electrons. At zero temperature the spins are ordered antiferromagnetically. Due to the strong localization of f states, the magnetic coupling between Ln ions is very weak, leading to very low Néel temperature for all Ln_2O_3 (lower than 10 K).[4] Therefore at room temperature all Ln_2O_3 are found in the disordered paramagnetic phase. Due to its lack of long-range order, the paramagnetic (PM) phase is difficult to treat in first-principles approaches. In the literature the PM phase is sometimes modeled by the nonmagnetic (NM) (spin-unpolarized) phase. This is justified only for metallic PM systems whose magnetic moment is attributed to the spin of itinerant electrons. For systems like Ln_2O_3, where the magnetic moment arises from strong local electron-electron interactions and persists even in the PM phase, the nonmagnetic state cannot be used to represent the PM phase. Fluctuations of the local spin moment have to be taken into account to rigorously treat the PM phase. This is possible in model-Hamiltonian-based approaches like DMFT,[20] but not in static mean-field theories like LDA or in the GW approach in its standard zero-temperature formalism. On the other hand, the magnetic order and the electronic band structure involve different degrees of freedom and different energy scales. One can therefore expect that the coupling between them should be weak. That the LDA gives dramatically different descriptions for the ferromagnetic (FM) and antiferromagnetic (AFM) phase for later transition-metal oxides[95] can be mainly attributed to the failure of LDA. To demonstrate this point, we use Ce_2O_3 as an example to investigate the effects of the magnetic order on the electronic band structure. For Ce_2O_3, the FM phase is energetically only 64 meV per formula unit less favorable than the AFM phase based on LDA + U calculations with $U = 5.44$ eV, which is consistent with the rather low Néel temperature (∼7 K) observed experimentally.[96]

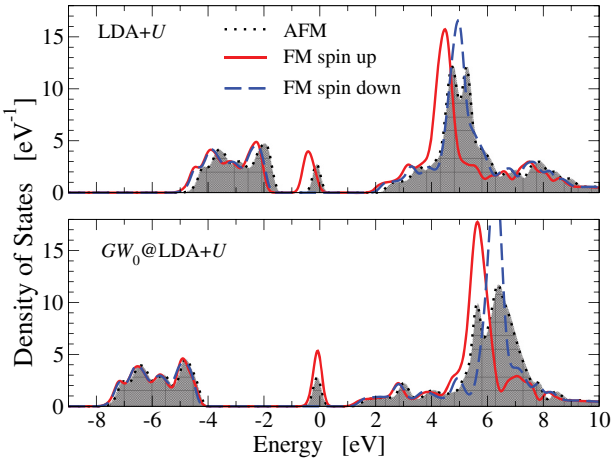

FIG. 3. (Color online) Density of states of Ce_2O_3 from LDA + U and GW_0@LDA + U in the ferromagnetic and antiferromagnetic phases. The spin-up and -down DOS in the AFM phase are identical, and therefore only one is shown.

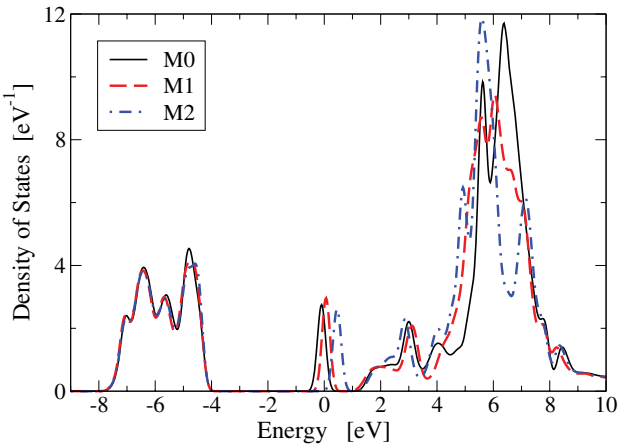

FIG. 4. (Color online) Density of states of Ce_2O_3 from GW_0@LDA + U with $U = 5.4$ eV in different metastable states. To see the differences more clearly, the data from M1 and M2 are shifted horizontally by 0.15 and 0.6 eV, respectively, so that the upper edges of their O-2p valence band match that of M0.

Figure 3 shows the spin-dependent DOS for the FM and AFM phases of Ce_2O_3 from LDA + U and GW_0@LDA + U. We can see clearly that the features arising from itinerant states in the two spin channels are nearly identical in both LDA + U and GW_0, further confirming that the highly localized 4f states interact only weakly with the itinerant states. The f^{occ} peak is present only in the spin majority DOS. The positions of the f^{un} states in the two spin channels differ by ∼0.7 eV due to the different exchange interaction.

The most striking feature in Fig. 3 is the similarity between the FM and AFM phases in both LDA + U and GW. While there are still some noticeable differences between the two phases in LDA + U, the main features of the two phases in GW_0@LDA + U are nearly identical. From this we conclude that the magnetic order indeed has a weak effect on the electronic band structure of systems like the lanthanide oxides with highly localized f states. Hence it is reasonable to approximate the DOS of the paramagnetic phase by that of the AFM (zero-temperature) phase. For the remainder, we therefore consider only the AFM phase. We note, however, that neither LDA + U nor G_0W_0@LDA + U can describe the phase transition between the AFM and the PM phases.

C. Ground and metastable states

An important issue in LDA + U calculations for open d or f shells is the presence of several local minima in the DFT self-consistency cycle.[32,97,98] As a result, it is often not straightforward to find the global minimum of the LDA + U total energy, a problem that has been known in the Hartree-Fock community for a while.[99–101] In this work, we try to locate the global minimum for each oxide by starting LDA + U calculations with randomly initialized density matrices for the local manifold and repeat the calculation ∼20 times. The resulting local minima correspond to different occupations of the open f shell. The question then is how different these metastable states are from the true ground state in terms of their electronic band structure? We will use Ce_2O_3 as an example to investigate this issue.

Three stable insulating states, denoted M0, M1, and M2, are found for Ce_2O_3 in the AFM phase. M1 and M2 are 0.56 and 0.81 eV per formula unit less stable than M0. Several metallic metastable states are also found at significantly higher energies, and are therefore not considered here. The LDA + U band gaps for M0, M1, and M2 are 2.24, 1.67, and 1.66 eV, respectively, and the corresponding GW_0 values 1.29, 0.94, and 0.64 eV. Figure 4 shows the band structure for the three metastable states in GW_0@LDA + U. By aligning all curves at the upper edge of the O-2p states, we can clearly see that the band structure mainly differs for features derived from localized f states. Features related to the itinerant bands (O-2p, Ce-5d) including, in particular, the p-d gap, are nearly identical. This can be attributed to the different occupation of the f states, which leads to slightly different interactions between itinerant and localized states. The itinerant bands are barely affected by this, due to the rather weak coupling between localized and itinerant states.

On the one hand, a careful search for the ground state is important for an accurate treatment of systems with open f shells, in particular if some metastable states exhibit a different behavior (e.g., metallic vs insulating). The example of Ce_2O_3, on the other hand, shows that the lowest-lying metastable states are all insulating and have a similar band structure. We note in addition that the presence of metastable states with similar energy is related to the multiplet structure of localized f states, which has been recently shown to play a significant role in determining the electronic structure of rare-earth materials.[97,102]

D. Comparison of G_0W_0 and GW_0

In this work, we mainly present results from the GW_0@LDA + U approach, in contrast to our previous work in which G_0W_0 was used. The main difference of GW_0 with respect to G_0W_0 is that the Green's function G is calculated self-consistently using quasiparticle energies. However, the QP wave functions are still approximated by KS ones, and the screened Coulomb interaction W is frozen at the W_0 level.

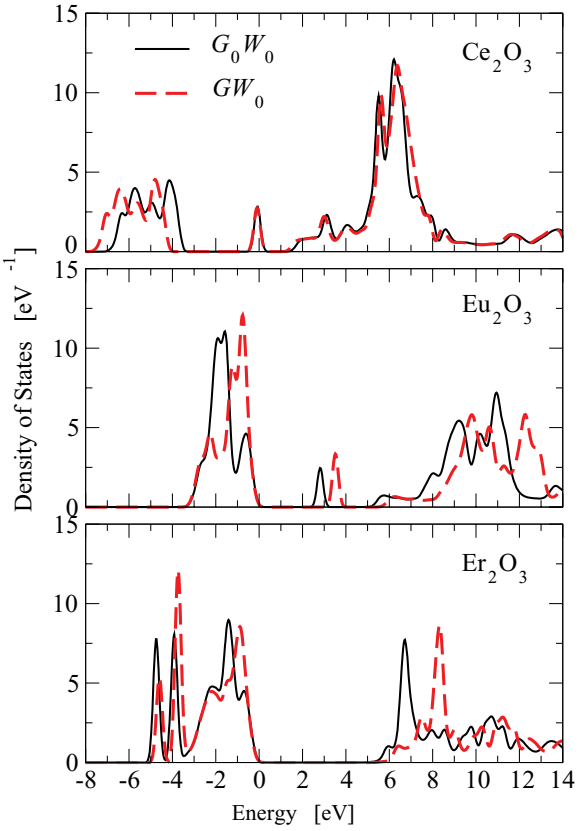

FIG. 5. (Color online) Density of states of Ce_2O_3, Eu_2O_3, and Er_2O_3 from G_0W_0 and GW_0@LDA + U.

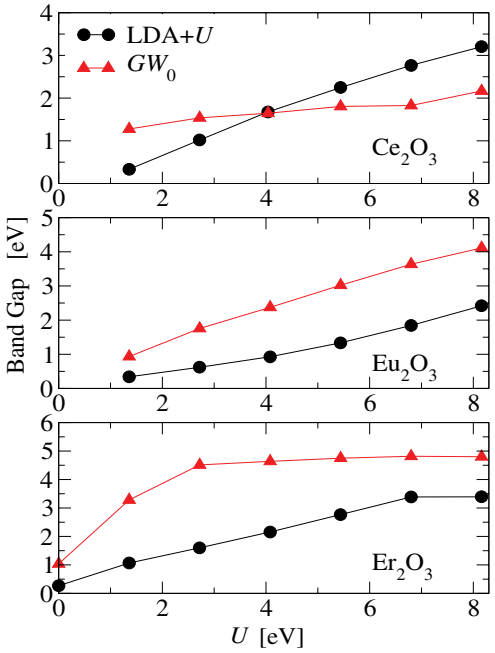

FIG. 6. (Color online) The band gaps of Ce_2O_3, Eu_2O_3, and Er_2O_3 from LDA + U and GW_0@LDA + U as a function of U.

For typical semiconductors, GW_0 often produces band gaps in better agreement with experiment than G_0W_0.[71,91] GW_0 results are also found to be very close to those from much more sophisticated quasiparticle self-consistent GW calculations in which an explicit treatment of the electron-hole interaction is included in W.[72] In physical terms, the good performance of GW_0 can be attributed to an error cancellation between neglecting full self-consistency and omitting the missing electron-hole (vertex correction) interaction in W.[71] The screened Coulomb interaction in RPA tends to be underscreened if it is calculated self-consistently, which would be compensated in an exact treatment by the additional screening provided by vertex corrections beyond RPA.

Due to the lack of reliable experimental data across the lanthanide series and the absence of accurate theoretical benchmark results, it is not easy to establish the performance of GW_0 for f-electron systems. We therefore content ourselves with a comparison between G_0W_0 and GW_0 for three distinct cases, whose band gaps have f-d, p-f, and p-d character. Figure 5 shows GW_0 and G_0W_0 DOS of Ce_2O_3, Eu_2O_3, and Er_2O_3. The overall shape of the spectra is similar, but several differences are noteworthy: (1) the p-d gaps from GW_0 are larger by ~0.5 eV; (2) the $f^{\rm occ}$ states are shifted towards higher energy with respect to the O-2p valence band; and (3) the $f^{\rm un}$ states have nearly the same energy in Ce_2O_3 with respect to the bottom of the Ln-5d conduction band, but are shifted towards considerably higher energies in Eu_2O_3 and Er_2O_3. The first feature is similar to that in sp semiconductors, i.e., GW_0 tends to give larger band gaps than G_0W_0. Aside from that, partial self-consistency has a different effect on itinerant and localized states so that the position of the $f^{\rm occ}$ and $f^{\rm un}$ states with respect to the itinerant bands changes quite significantly.

E. Dependence on U

In our previous work,[19] we have shown that G_0W_0@LDA + U is less sensitive to U than LDA + U in CeO_2 and Ce_2O_3. Here we extend this analysis to other compounds in the series. Figures 6 and 7 show once more that LDA + U and GW_0@LDA + U exhibit a different U dependence. In contrast to GW_0@LDA + U, band gaps in LDA + U change linearly with U when the highest occupied states and/or lowest unoccupied states are mainly of f character. The difference in DOS is even more pronounced. In all three materials of Fig. 7, $f^{\rm occ}$ states are pushed to lower energies in LDA + U as U increases, while GW reverses this downwards shift. This is analogous to the behavior of GW@LDA + U observed for semicore d states in ZnS.[61,62,71] In general, the dependence on U in GW_0@LDA + U is much weaker than in LDA + U.

It is evident from Figs. 6 and 7 that the three materials exhibit a rather different U dependence, which can be explained by their different band characteristics. As we have emphasized previously for d-electron systems,[62] the influence of U in GW@LDA + U manifests itself indirectly through the change of the screening strength and the change of the LDA + U wave functions. Since the LDA + U band gap always increases with U, screening decreases, which contributes to increasing the GW band gap. On the other hand, increasing U not only shifts the positions of $f^{\rm occ}$ and $f^{\rm un}$ states, but also changes the hybridization between localized (Ln-4f) and itinerant (O-2p and Ln-5d) states which affects the single-particle wave functions. The wave-function change might decrease or increase the GW band gap, depending on the character of the highest occupied (HO) and the lowest unoccupied (LU)

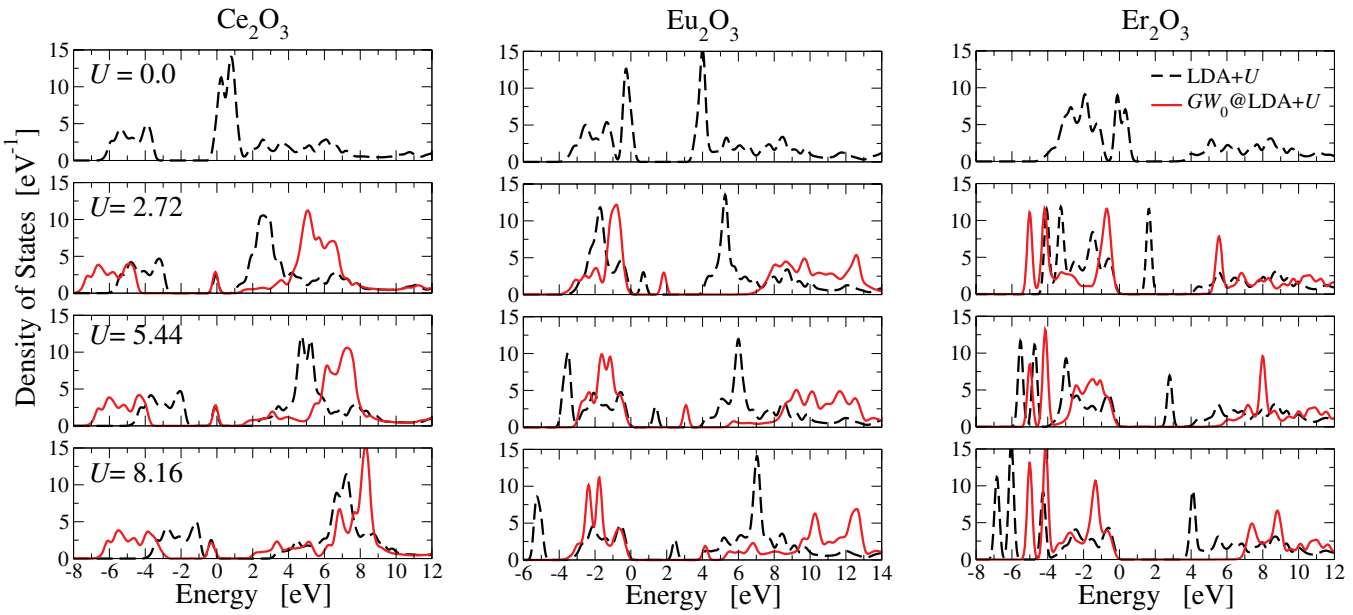

FIG. 7. (Color online) Density of states of Ce_2O_3, Eu_2O_3, and Er_2O_3 from LDA + U and GW_0@LDA + U with different U (in units of eV).

state. Here the tendency is opposite, while a more localized HO state reduces the band gap, the LU has to become more delocalized to have the same effect.[62] In Ce_2O_3, the highest occupied states are mainly of Ce-4f character through the whole range of U investigated, but the lowest unoccupied states evolve from mainly Ce-4f (more localized) character in LDA to dominantly Ce-5d (more delocalized) at large U. This decreases the band gap as U increases. The two factors (screening and hybridization) cancel each other, leading to an overall weak U dependence. In Eu_2O_3, the LU states in LDA + U are predominantly Eu-4f, whereas the HO states become more delocalized as the Eu-f^{occ} states are pushed towards lower energy at larger U. Therefore both factors tend to increase the band gap as U increases, leading to a strong U dependence in GW@LDA + U. In Er_2O_3, the situation is more complicated. As U increases, the HO states evolve from having a significant Er-4f contribution at small U to mainly O-2p (itinerant) character at large U, whereas the LU states transition from Er-4f character to Er-5d character. This explains the fact that the GW band gap increases rapidly at small U, but flattens out at large U.

Another distinct feature in Fig. 7 is the fact that f-derived peaks in LDA + U are sharper than in GW_0@LDA + U. This is mainly an artifact of approximating QP wave functions by LDA + U ones. Considering that the size of the GW corrections depends strongly on the character (localized vs itinerant) of the state, the difference between true QP wave functions and KS wave functions is likely to be much larger for those with strong f character than for normal itinerant states, and therefore significant state mixing[103] is expected.

F. Systematic trends across the Ln_2O_3 series

In Ref. 19, we found that G_0W_0 based on LDA + U, without any empirical adjustment of the Hubbard U, reproduces all main features in the experimental optical band gap vs compound curve. The characteristic variation of the band gaps is caused by a systematic change in the position of occupied and unoccupied f states with respect to the edges of the itinerant bands. In this section we will elucidate this behavior in more detail. The band gaps of Ln_2O_3 obtained from LDA + U, G_0W_0 and GW_0 are collected in Table I together with available experimental data, and are visualized in Fig. 8.

The variation of the optical band gaps across the Ln_2O_3 series is nonmonotonic and gives rise to the term "small periodic systems of the lanthanide."[104] The variation of the band gaps in the first and second half of the series is strikingly

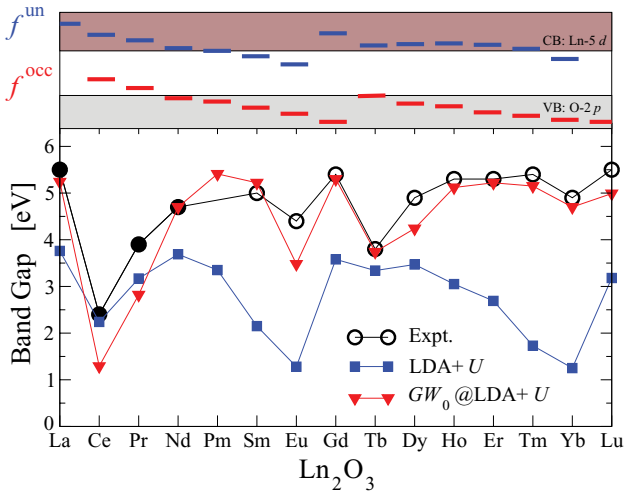

FIG. 8. (Color online) Band gaps of the whole Ln_2O_3 series from LDA + U and GW_0@LDA + U are compared to experimental band gaps obtained from optical absorption (Ref. 104). Experimental values of compounds that crystallize preferentially in the hexagonal structure are denoted by filled circles. The upper part of the figure illustrates the position of occupied and unoccupied 4f states with respect to the valence and conduction bands schematically. A more complete comparison between different theoretical approaches and experiment is presented in Table I.

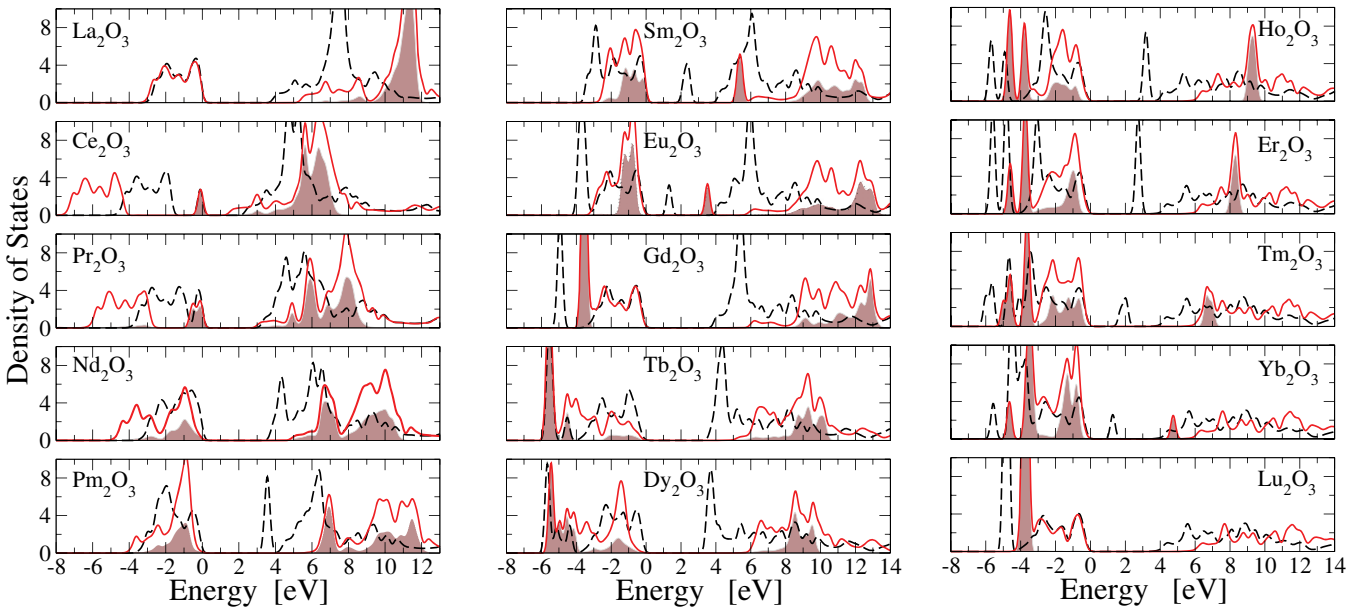

FIG. 9. (Color online) Density of states of the Ln_2O_3 series from LDA + U (dashed lines) and GW_0@LDA + U (solid lines). The shaded regions illustrate the Ln-4f character in the GW_0 DOS.

similar. The band gaps of Ce_2O_3, Eu_2O_3, Tb_2O_3, and Yb_2O_3 are significantly smaller than their neighbors (four dips in the plot) while the La, Gd, Ho, Er, Tm, and Lu oxides have nearly the same band gap. These features are well reproduced by G_0W_0 and GW_0 based on LDA + U,[19] whereby GW_0 is in better quantitative agreement with experiment. The remaining differences could be due to several factors. (1) GW is an approximate self-energy. (2) The experimental band gaps are obtained from optical absorption, which will include excitonic and polaronic effects that are not taken into account in our calculations. Also, the determination of the absorption edge is not unambiguous, which introduce additional uncertainty (error bars) in optical band gaps. (3) As we have discussed in Sec. III A, the lanthanide sesquioxides exist in several polymorphs, and only the light members of the series crystallize in the hexagonal structure that is considered in our calculations. The comparison is further aggravated by the fact that the crystal structures used for the optical measurements are not reported in Ref. 104. (4) For compounds with a p-f or f-d gap, the spin-orbit coupling, which is not considered in our work, may also play a role.

The variation of the Ln_2O_3 band gap can be understood in terms of the f-state position as the number of f electrons increases. Based on phenomenological considerations derived from high-temperature conductivity measurements, Lal and Gaur partitioned the Ln_2O_3 series into three categories.[108] (a) For La, Gd, Dy, Ho, and Er, both $f^{\rm occ}$ and $f^{\rm un}$ bands lie outside the p-d band gap. (b) For Ce, Pr, Nd, and Tb, the $f^{\rm occ}$ band falls within the p-d gap, and $f^{\rm un}$ lies above the Ln-5d conduction-band minimum (CBM), and (c) for Sm, Eu, Tm and Yb, the $f^{\rm occ}$ band lies below the O-2p valence-band maximum (VBM), and $f^{\rm un}$ falls within the p-d gap. Case "d" in Ref. 108, in which both $f^{\rm occ}$ and $f^{\rm un}$ bands fall within the p-d gap does not occur for the Ln_2O_3 series. In their comprehensive analysis of the optical gaps of the Ln_2O_3 series, Prokofiev *et al.* proposed a similar band model but with different classifications for Sm, Eu, Tm, and Yb, which were all assigned to case "a." To determine the position of the $f^{\rm occ}$ and $f^{\rm un}$ states in our calculations, we plot in Fig. 9 the DOSs of the whole Ln_2O_3 series obtained from LDA + U and GW_0. The gray shaded areas mark the local density of states projected onto the Ln-4f orbitals. From La to Gd the $f^{\rm occ}$ and $f^{\rm un}$ states continuously move down in energy, as the number of f electrons in the spin-majority channel increases. The nature of the minimal gap varies accordingly from p-d to f-d to p-f. In the second half of the series the process repeats itself as the spin-minority f shell is filled.[62]

In La_2O_3 the 4f states are empty and the band gap is of p-d type. The $f^{\rm un}$ peak resides at approximately 6 eV above the CBM. In Ce_2O_3 and Pr_2O_3, the $f^{\rm occ}$ peak is well separated from the O-2p valence band and falls within the p-d gap. In Nd_2O_3, the $f^{\rm occ}$ peak nearly merges with the O-2p valence band, but the highest occupied states are still mainly of Nd-4f character. GW_0 therefore predicts that the minimal gap in Ce_2O_3, Pr_2O_3, and Nd_2O_3 is of f-d character, which agrees with the experimental conjecture derived from both optical absorption[104] and high-temperature conductivity measurements.[108] Compared to the experimental optical gaps, the GW_0 band gaps of Ce_2O_3 and Pr_2O_3 are underestimated by around 1 eV, which is likely due to the fact that GW tends to underestimate the binding energy of localized states significantly.[19,71,72] In the next three members of the series, Pm_2O_3, Sm_2O_3, and Eu_2O_3, the $f^{\rm occ}$ states overlap with the O-2p valence band. The lowest $f^{\rm un}$ states reside at the bottom of the conduction band in Pm_2O_3 and Sm_2O_3 and are pulled into the p-d gap in Eu_2O_3. Eu_2O_3 therefore has a p-f gap, but for Pm_2O_3 and Sm_2O_3 the assignment is more subtle. According to the GW_0 DOS, they should be categorized as p-f (i.e., case "c"). On the other hand, since the Ln-5d states are much more delocalized than the 4f states, optical transitions

from the O-2p to the Ln-5d states should have a much larger cross section. Optical-absorption experiments would therefore very likely point to a p-d gap even though the $f^{\rm un}$ states lie at lower energy than the Ln-5d states. This is probably the reason for the different assignments in optical-absorption[104] and high-temperature conductivity[108] experiments for Sm_2O_3.

In Gd_2O_3, the spin majority f shell is fully occupied, and the spin minority f shell is empty. The $f^{\rm occ}$ peak now falls below the O-2p valence band, and the $f^{\rm un}$ states in the conduction band. As the spin-minority f shell is filled one by one, a trend that is similar to the first half of the series follows, except that the $f^{\rm occ}$ states of spin minority move down in energy more quickly. Even in Tb_2O_3, the counterpart to Ce_2O_3, the $f^{\rm occ}$ already merges with the O-2p valence band. On the other hand, the $f^{\rm un}$ states now move to lower energy "more slowly." Even for Yb_2O_3, the $f^{\rm un}$ peak falls just below the CBM, which gives Yb_2O_3 a considerably larger band gap than Eu_2O_3.

Due to its promising role as a high-κ material, Lu_2O_3 has attracted a lot of interest in recent years.[107,109] The band gap is a critical parameter for high-κ candidates since it has to be large enough to provide hole and electron barriers to silicon. The band gaps of Lu_2O_3 obtained from optical-absorption studies are highly scattered and span a range of 4.9–5.8 eV.[104,105,107] Internal photoemission spectroscopy[107] gives a band gap of 5.8 eV. In GW_0@LDA + U the band gap amounts to only 5.0 eV, which is surprising considering that Lu_2O_3 has a p-d-type gap that should be well described by GW_0. Apart from the factors we have discussed before, a likely cause of this discrepancy is the low density of states at the bottom of the conduction band originating from highly dispersive Lu-6s states. The GW_0 DOS of Lu_2O_3 in Fig. 9 shows a steep rise at about 6 eV, although the minimal band gap is at much lower energy (∼5.0 eV). The internal photoemission experiment may have difficulties to capture this feature so that a unique determination of the band edge becomes difficult,[110] which may also explain the wide scatter of the experimental data.

IV. COMPARISON TO DMFT

In this section we make a comparison between GW and DMFT.[20] The latter, usually combined with an LDA description of the itinerant states, is often regarded as the method of choice for strongly correlated systems and can treat paramagnetic systems directly. As we have pointed out previously,[19] both GW@LDA + U and LDA + DMFT recover correlation effects that are missing in LDA + U. GW@LDA + U does so by using LDA + U as the reference and expanding the xc self-energy correction with respect to the dynamically screened Coulomb interaction W to first order. This has the advantage that all states, both localized and itinerant ones, are corrected with respect to LDA, but the disadvantage that all interactions are treated at the GW level. For highly localized electrons this may not be sufficient. LDA + DMFT, on the other hand, introduces higher-order interactions among localized states in a way that is exact in the limit of infinite dimension. The fact that these, in practice, are limited to the local manifold is an obvious limitation. In addition, DMFT calculations are currently restricted to relatively high temperatures for computational reasons. To overcome the drawbacks of LDA, Jacob *et al.* recently proposed to use hybrid functionals instead.[22]

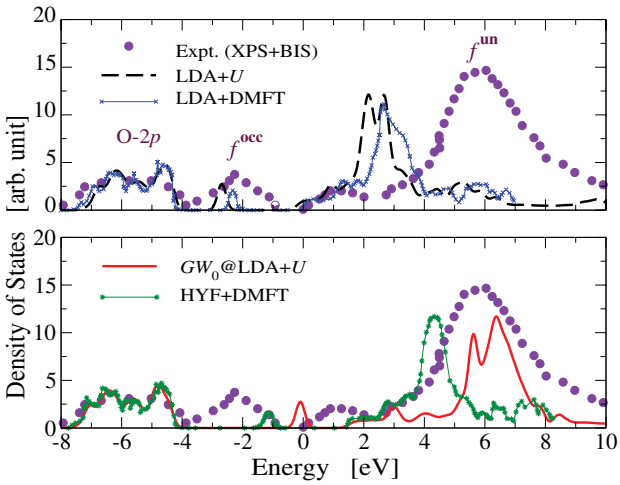

FIG. 10. (Color online) Density of states of Ce_2O_3 in LDA + U, GW_0@LDA + U, LDA + DMFT with self-consistency in the charge density [LDA + DMFT(SC)] (Ref. 23), and the hybrid density functional plus DMFT approach (HYF + DMFT) (Ref. 22) as well as experimental spectral data from XPS + BIS (Ref. 111), all aligned at the upper edge of the O-2p valence band. We note that the small peak ∼3 eV above $f^{\rm occ}$ in the XPS + BIS data is likely due to unoccupied f states of CeO_2 contamination in the Ce_2O_3 sample as evidenced by Fig. 3 in Ref. 111. The edge of the conduction band can therefore be estimated to appear at around 4 eV above the $f^{\rm occ}$ peak, which then gives an experimental p-d gap of ∼6 eV.

To illustrate the comparison more clearly, we consider Ce_2O_3, for which several DMFT studies have been performed.[22,23] In Fig. 10 the LDA + U and GW_0@LDA + U densities of states of Ce_2O_3 are compared to those from LDA + DMFT with self-consistency in the charge density,[23] and from DMFT in combination with the hybrid functional DFT (HYF + DMFT).[22] Experimental data from x-ray photoemission spectroscopy (XPS) and bremsstrahlung-isochromat spectroscopy (BIS) are also shown for comparison.[111] All spectra are aligned at the upper edge of the O-2p valence band. We note that such an alignment is necessary because the absolute energy scale in our bulk calculations is arbitrary. Since the O-2p valence band is experimentally a well defined feature, it is meaningful to use its upper edge for the alignment.

The DOS in LDA + U and LDA + DMFT is very similar except for some slight differences in the positions of the $f^{\rm occ}$ and $f^{\rm un}$ states. Both describe the position of the $f^{\rm occ}$ states with respect to the O-2p valence band rather well, but the position of the $f^{\rm un}$ states differs from experiment dramatically, by as much as 4 eV. Another remarkable failure of both LDA + U and LDA + DMFT is the significant underestimation of the p-d gap. GW_0@LDA + U and HYF + DMFT give a similar description for the itinerant states, but differ for the $f^{\rm occ}$ and $f^{\rm un}$ states. In particular, the $f^{\rm un}$ peak is ∼2 eV higher in GW_0@LDA + U, in better agreement with experiment compared to HYF + DMFT. Although the combination between HYF and DMFT improves the description of itinerant states, the interaction between localized and itinerant states is still

treated at the HYF level. The latter may not be enough since the exchange-correlation potential in HYF depends on occupied states only and may thus still have difficulties in treating unoccupied states accurately.

The comparison between GW@LDA$+U$ and DMFT for Ce_2O_3 indicates that combining DMFT with a static mean-field theory like HYF will likely not be sufficient to describe all features of the electronic structure of f-electron systems correctly. The GW approach, on the other hand, suffers from an underestimation of the binding energy of occupied d and f states[19,62] and the absence of satellites.[62] These limitations have been attributed to higher-order short-range correlation effects that are missing in the GW approximation. The latter are likely to be stronger for more localized states.[39,72] Naturally we expect that combining GW with DMFT may provide the best choice: GW can not only describe itinerant states more accurately, but can also be used to determine, in a first-principles manner, the effective Hubbard interaction parameters in the framework of the constrained random-phase approximation.[75] On the other hand, vertex corrections constructed from DMFT, which will improve the descriptions of localized d or f states, can in principle also be incorporated into the GW framework.[21,112,113] Preliminary work in this direction, mainly based on model systems, has been very promising,[112,113] but substantial work is still needed to implement the approach for real systems.

V. CONCLUSIONS

In this paper we have presented a systematic investigation of the electronic band structure of lanthanide sesquioxides using the GW@LDA$+U$ approach. The influence of the crystal structure, the magnetic order, and the existence of metastable states has been studied. Each introduce noticeable effects in the density of states, but the overall features remain unchanged. The dependence on U has been investigated for Ce_2O_3, Eu_2O_3, and Er_2O_3 as typical cases whose minimal band gaps are of f-d, p-f, and p-d character. We found the dependence to be relatively weak in Ce_2O_3 and Er_2O_3, but strong in Eu_2O_3, which can be understood in terms of the effects of U on changing the screening strength and the character of the highest occupied and lowest unoccupied bands. We have further discussed the systematic evolution of the electronic band structure of the whole Ln_2O_3 series. The characteristic features observed for the optical band gaps of the series are well reproduced by GW_0@LDA$+U$, and are caused mainly by the continual shift of the f states towards lower energy with respect to itinerant bands as the number of f electrons increases. We have made a preliminary comparison between GW@LDA$+U$ and DMFT, the latter being combined with LDA or a hybrid functional, using our results and those published in the literature for Ce_2O_3, which indicates that a combining GW with DMFT might be the best choice for strongly correlated semiconducting or insulating systems like lanthanide oxides.

ACKNOWLEDGMENTS

This work was in part funded by National Natural Science Foundation of China (Project No. 20973009) and the EU's Sixth Framework Programme through the NANOQUANTA (NMP4-CT-2004-500198) network of excellence and the EU's Seventh Framework Programme through European Theoretical Spectroscopy Facility e-Infrastructure Grant No. 211956. P. Rinke acknowledges the support of the Deutsche Forschungsgemeinschaft.

*Author to whom correspondence should be addressed: h.jiang@pku.edu.cn

[1] *Handbook on the Physics and Chemistry of Rare Earths*, edited by K. A. Gschneidner and L. Eyring (North-Holland, Amsterdam, 1978–2010), Vols. 1–40.

[2] S. Y. Savrasov, G. Kotliar, and E. Abrahams, Nature (London) **410**, 793 (2001).

[3] L. Eyring, *The Binary Rare Earth Oxides*, Handbook on the Physics and Chemistry of Rare Earths No. 3 (North-Holland, Amsterdam, 1979), Chap. 27, p. 337.

[4] G. Adachi and N. Imanaka, Chem. Rev. **98**, 1479 (1998).

[5] A. Trovarelli, *Catalysis by Ceria and Related Materials* (Imperial College Press, London, 2002).

[6] *Rare Earth Oxide Thin Films: Growth, Characterization and Applications*, Topics in Applied Physics No. 106, edited by M. Fanciulli and G. Scarel (Springer, Heidelberg, 2007).

[7] D. G. Schlom, S. Guha, and S. Datta, MRS Bull. **33**, 1017 (2008).

[8] D. D. Koelling, A. M. Boring, and J. H. Wood, Solid State Commun. **47**, 227 (1983).

[9] N. V. Skorodumova, R. Ahuja, S. I. Simak, I. A. Abrikosov, B. Johansson, and B. I. Lundqvist, Phys. Rev. B **64**, 115108 (2001).

[10] P. J. Hay, R. M. Martin, J. Uddin, and G. E. Scuseria, J. Chem. Phys. **125**, 034712 (2006).

[11] D. A. Andersson, S. I. Simak, B. Johansson, I. A. Abrikosov, and N. V. Skorodumova, Phys. Rev. B **75**, 035109 (2007).

[12] C. Loschen, J. Carrasco, K. M. Neyman, and F. Illas, Phys. Rev. B **75**, 035115 (2007).

[13] J. L. F. Da Silva, M. V. Ganduglia-Pirovano, J. Sauer, V. Bayer, and G. Kresse, Phys. Rev. B **75**, 045121 (2007).

[14] J. L. F. Da Silva, Phys. Rev. B **76**, 193108 (2007).

[15] N. Hirosaki, S. Ogata, and C. Kocer, J. Alloys Compd. **351**, 2003 (2003).

[16] B. Wu, M. Zinkevich, F. Aldinger, D. Wen, and L. Chen, J. Solid State Chem. **180**, 3280 (2007).

[17] L. Petit, A. Svane, Z. Szotek, and W. M. Temmerman, Phys. Rev. B **72**, 205118 (2005).

[18] L. Hedin, Phys. Rev. A **139**, 796 (1965).

[19] H. Jiang, R. I. Gomez-Abal, P. Rinke, and M. Scheffler, Phys. Rev. Lett. **102**, 126403 (2009).

[20] G. Kotliar, S. Y. Savrasov, K. Haule, V. S. Oudovenko, O. Parcollet, and C. A. Marianetti, Rev. Mod. Phys. **78**, 865 (2006).

[21] K. Held, Adv. Phys. **56**, 829 (2007).

[22]D. Jacob, K. Haule, and G. Kotliar, Europhys. Lett. **84**, 57009 (2008).
[23]L. V. Pourovskii, B. Amadon, S. Biermann, and A. Georges, Phys. Rev. B **76**, 235101 (2007).
[24]R. G. Parr and W. Yang, *Density-Functional Theory of Atoms and Molecules* (Oxford University Press, New York, 1989).
[25]R. M. Dreizler and E. K. U. Gross, *Density Functional Theory: An Approach to the Quantum Many-Body Problem* (Springer-Verlag, Berlin, 1990).
[26]R. M. Martin, *Electronic Structure: Basic Theory and Practical Methods* (Cambridge University Press, Cambridge, UK, 2004).
[27]A. D. Becke, J. Chem. Phys. **98**, 1372 (1993).
[28]J. P. Perdew, M. Ernzerhof, and K. Burke, J. Chem. Phys. **105**, 9982 (1996).
[29]M. Marsman, J. Paier, A. Stroppa, and G. Kresse, J. Phys.: Condens. Matter **20**, 064201 (2008).
[30]T. M. Henderson, J. Paier, and G. E. Scuseria, Phys. Status Solidi B **248**, 767 (2011).
[31]K. N. Kudin, G. E. Scuseria, and R. L. Martin, Phys. Rev. Lett. **89**, 266402 (2002).
[32]F. Jollet, G. Jomard, B. Amadon, J. P. Crocombette, and D. Torumba, Phys. Rev. B **80**, 235109 (2009).
[33]V. Eyert, Phys. Rev. Lett. **107**, 016401 (2011).
[34]V. I. Anisimov, I. V. Solovyev, M. A. Korotin, M. T. Czyzyk, and G. A. Sawatzky, Phys. Rev. B **48**, 16929 (1993).
[35]V. I. Anisimov, F. Aryasetiawan, and A. I. Lichtenstein, J. Phys.: Condens. Matter **9**, 767 (1997).
[36]W. G. Aulbur, L. Jönsson, and J. W. Wilkins, Solid State Phys. **54**, 1 (2000).
[37]P. Rinke, A. Qteish, J. Neugebauer, and M. Scheffler, Phys. Status Solidi B **245**, 929 (2008).
[38]F. Aryasetiawan, Phys. Rev. B **46**, 13051 (1992).
[39]F. Aryasetiawan and O. Gunnarsson, Phys. Rev. Lett. **74**, 3221 (1995).
[40]F. Aryasetiawan and K. Karlsson, Phys. Rev. B **54**, 5353 (1996).
[41]S. Massidda, A. Continenza, M. Posternak, and A. Baldereschi, Phys. Rev. B **55**, 13494 (1997).
[42]A. Yamasaki and T. Fujiwara, Phys. Rev. B **66**, 245108 (2002).
[43]S. V. Faleev, M. van Schilfgaarde, and T. Kotani, Phys. Rev. Lett. **93**, 126406 (2004).
[44]J.-L. Li, G.-M. Rignanese, and S. G. Louie, Phys. Rev. B **71**, 193102 (2005).
[45]C. H. Patterson, Int. J. Quantum Chem. **106**, 3383 (2006).
[46]F. Bruneval, N. Vast, L. Reining, M. Izquierdo, F. Sirotti, and N. Barrett, Phys. Rev. Lett. **97**, 267601 (2006).
[47]A. N. Chantis, M. van Schilfgaarde, and T. Kotani, Phys. Rev. B **76**, 165126 (2007).
[48]M. Gatti, F. Bruneval, V. Olevano, and L. Reining, Phys. Rev. Lett. **99**, 266402 (2007).
[49]C. Rödl, F. Fuchs, J. Furthmüller, and F. Bechstedt, Phys. Rev. B **77**, 184408 (2008).
[50]T. Kotani, M. van Schilfgaarde, and S. V. Faleev, Phys. Rev. B **76**, 165106 (2007).
[51]A. N. Chantis, R. C. Albers, M. D. Jones, M. van Schilfgaarde, and T. Kotani, Phys. Rev. B **78**, 081101(R) (2008).
[52]R. Sakuma, T. Miyake, and F. Aryasetiawan, Phys. Rev. B **78**, 075106 (2008).
[53]S. Kobayashi, Y. Nohara, S. Yamamoto, and T. Fujiwara, Phys. Rev. B **78**, 155112 (2008).
[54]C. Rödl, F. Fuchs, J. Furthmüller, and F. Bechstedt, Phys. Rev. B **79**, 235114 (2009).
[55]Y. Nohara, S. Yamamoto, and T. Fujiwara, Phys. Rev. B **79**, 195110 (2009).
[56]R. Sakuma, T. Miyake, and F. Aryasetiawan, Phys. Rev. B **80**, 235128 (2009).
[57]H. Jiang, Acta. Phys. Chim. Sin. **26**, 1017 (2010).
[58]J. H. Richter, B. J. Ruck, M. Simpson, F. Natali, N. O. V. Plank, M. Azeem, H. J. Trodahl, A. R. H. Preston, B. Chen, J. McNulty *et al.*, Phys. Rev. B **84**, 235120 (2011).
[59]P. Liao and E. A. Carter, PhysChemChemPhys **13**, 15189 (2011).
[60]M. C. Toroker, D. K. Kanan, N. Alidoust, L. Y. Isseroff, P. Liao, and E. A. Carter, PhysChemChemPhys **13**, 16644 (2011).
[61]T. Miyake, P. Zhang, M. L. Cohen, and S. G. Louie, Phys. Rev. B **74**, 245213 (2006).
[62]H. Jiang, R. I. Gomez-Abal, P. Rinke, and M. Scheffler, Phys. Rev. B **82**, 045108 (2010).
[63]Y. Zhang, X. Yuan, X. Sun, B.-C. Shih, P. Zhang, and W. Zhang, Phys. Rev. B **84**, 075127 (2011).
[64]L. Hedin and B. I. Lundqvist, Solid State Phys. **23**, 1 (1969).
[65]M. S. Hybertsen and S. G. Louie, Phys. Rev. B **34**, 5390 (1986).
[66]R. W. Godby, M. Schlüter, and L. J. Sham, Phys. Rev. B **36**, 6497 (1987).
[67]F. Aryasetiawan and O. Gunnarsson, Rep. Prog. Phys. **61**, 237 (1998).
[68]G. Onida, L. Reining, and A. Rubio, Rev. Mod. Phys. **74**, 601 (2002).
[69]P. Rinke, A. Qteish, J. Neugebauer, C. Freysoldt, and M. Scheffler, New J. Phys. **7**, 126 (2005).
[70]F. Aryasetiawan, in *Strong Coulomb Correlations in Electronic Structure Calculations: Beyond the Local Density Approximation*, edited by V. I. Anisimov (Gordon and Breach, New York, 2000), p. 1.
[71]M. Shishkin and G. Kresse, Phys. Rev. B **75**, 235102 (2007).
[72]M. Shishkin, M. Marsman, and G. Kresse, Phys. Rev. Lett. **99**, 246403 (2007).
[73]P. H. Dederichs, S. Blügel, R. Zeller, and H. Akai, Phys. Rev. Lett. **53**, 2512 (1984).
[74]M. Cococcioni and S. de Gironcoli, Phys. Rev. B **71**, 035105 (2005).
[75]F. Aryasetiawan, M. Imada, A. Georges, G. Kotliar, S. Biermann, and A. I. Lichtenstein, Phys. Rev. B **70**, 195104 (2004).
[76]M. Aichhorn, L. Pourovskii, V. Vildosola, M. Ferrero, O. Parcollet, T. Miyake, A. Georges, and S. Biermann, Phys. Rev. B **80**, 085101 (2009).
[77]S. Fabris, S. de Gironcoli, S. Baroni, G. Vicario, and G. Balducci, Phys. Rev. B **71**, 041102(R) (2005).
[78]P. Blaha, K. Schwarz, G. K. H. Madsen, D. Kvasnicka, and J. Luitz, *WIEN2k, An Augmented Plane Wave + Local Orbitals Program for Calculating Crystal Properties* (Karlheinz Schwarz, Techn. Universität Wien, Austria, 2001).
[79]K. Schwarz, P. Blaha, and G. K. H. Madsen, Comput. Phys. Commun. **147**, 71 (2002).
[80]P. Novak, F. Boucher, P. Gressier, P. Blaha, and K. Schwarz, Phys. Rev. B **63**, 235114 (2001).
[81]R. Gomez-Abal, X. Li, M. Scheffler, and C. Ambrosch-Draxl, Phys. Rev. Lett. **101**, 106404 (2008).
[82]H. Jiang, R. Gomez-Abal, X. Li, C. Meisenbichler, C. Ambrosch-Draxl, and M. Scheffler (unpublished).

[83]H. N. Rojas, R. W. Godby, and R. J. Needs, Phys. Rev. Lett. **74**, 1827 (1995).
[84]W. E. Pickett, H. Krakauer, and P. B. Allen, Phys. Rev. B **38**, 2721 (1988).
[85]M. M. Rieger, L. Steinbeck, I. D. White, H. N. Rojas, and R. W. Godby, Comput. Phys. Commun. **117**, 211 (1999).
[86]C. Friedrich, M. C. Müller, and S. Blügel, Phys. Rev. B **83**, 081101(R) (2011).
[87]C. Friedrich, A. Schindlmayr, S. Blügel, and T. Kotani, Phys. Rev. B **74**, 045104 (2006).
[88]W.-K. Li, G.-D. Zhou, and T. C. W. Mak, *Advanced Structural Inorganic Chemistry* (Oxford University Press, New York, 2008).
[89]F. Fuchs and F. Bechstedt, Phys. Rev. B **77**, 155107 (2008).
[90]B. Králik, E. K. Chang, and S. G. Louie, Phys. Rev. B **57**, 7027 (1998).
[91]H. Jiang, R. I. Gomez-Abal, P. Rinke, and M. Scheffler, Phys. Rev. B **81**, 085119 (2010).
[92]V. Garbuio, M. Cascella, L. Reining, R. Del Sole, and O. Pulci, Phys. Rev. Lett. **97**, 137402 (2006).
[93]H. L. Yakel, Jr., Acta Crystallogr. Sect. B **35**, 564 (1979).
[94]Z. K. Heiba, Y. Akin, W. Sigmund, and Y. S. Hascicek, J. Appl. Crystallogr. **36**, 1411 (2003).
[95]K. Terakura, T. Oguchi, A. R. Williams, and J. Kübler, Phys. Rev. B **30**, 4734 (1984).
[96]H. Pinto, M. H. Mintz, M. Melamud, and H. Shaked, Phys. Lett. A **88**, 81 (1982).
[97]A. B. Shick, W. E. Pickett, and A. I. Liechtenstein, J. Electron Spectrosc. Relat. Phenom. **114–116**, 753 (2001).
[98]B. Meredig, A. Thompson, H. A. Hansen, C. Wolverton, and A. van de Walle, Phys. Rev. B **82**, 195128 (2010).
[99]H. Fukutome, Prog. Theor. Phys. **45**, 1382 (1971).
[100]M. D. de Andrade, K. C. Mundim, and L. A. C. Malbouisson, Int. J. Quantum Chem. **103**, 493 (2005).
[101]A. J. W. Thom and M. Head-Gordon, Phys. Rev. Lett. **101**, 193001 (2008).
[102]L. V. Pourovskii, K. T. Delaney, C. G. Van de Walle, N. A. Spaldin, and A. Georges, Phys. Rev. Lett. **102**, 096401 (2009).
[103]O. Pulci, F. Bechstedt, G. Onida, R. Del Sole, and L. Reining, Phys. Rev. B **60**, 16758 (1999).
[104]A. V. Prokofiev, A. I. Shelykh, and B. T. Melekh, J. Alloys Compd. **242**, 41 (1996).
[105]S. Kimura, F. Arai, and M. Ikezawa, J. Phys. Soc. Jpn. **69**, 3451 (2000).
[106]Y. Zhao, K. Kita, K. Kyuno, and A. Toriumi, Appl. Phys. Lett. **94**, 042901 (2009).
[107]G. Seguini, E. Bonera, S. Spiga, G. Scarel, and M. Fanciulli, Appl. Phys. Lett. **85**, 5316 (2004).
[108]H. B. Lal and K. Gaur, J. Mater. Sci. **23**, 919 (1988).
[109]V. V. Afanas'ev, M. Badylevich, A. Stesmans, A. Laha, H. J. Osten, A. Fissel, W. Tian, L. F. Edge, and D. G. Schlom, Appl. Phys. Lett. **93**, 192105 (2008).
[110]A. Schleife, J. B. Varley, F. Fuchs, C. Rödl, F. Bechstedt, P. Rinke, A. Janotti, and C. G. Van de Walle, Phys. Rev. B **83**, 035116 (2011).
[111]J. W. Allen, J. Magn. Magn. Mater. **47/48**, 168 (1985).
[112]S. Biermann, F. Aryasetiawan, and A. Georges, Phys. Rev. Lett. **90**, 086402 (2003).
[113]P. Sun and G. Kotliar, Phys. Rev. Lett. **92**, 196402 (2004).